Analog Multitone with Interference Suppression: Relieving the ADC Bottleneck for Wideband 60 GHz Systems

Hong Zhang, Sriram Venkateswaran and Upamanyu Madhow
Department of Electrical and Computer Engineering
University of California, Santa Barbara
Email: {hongzhang, sriram, madhow}@ece.ucsb.edu

***Abstract*—Commercial exploitation of the large amounts of unlicensed spectrum available at 60 GHz requires that we take advantage of the low-cost digital signal processing (DSP) made available by Moore's law. A key bottleneck, however, is the cost and power consumption of high-precision analog-to-digital converters (ADCs) at the multiGigabit rates of interest in this band. This makes it difficult, for example, to apply traditional DSP-based approaches to channel dispersion compensation such as time domain equalization or Orthogonal Frequency Division Multiplexing (OFDM), since these are predicated on the availability of full-rate, high-precision samples. In this paper, we investigate the use of analog multitone for sidestepping the ADC bottleneck: transmissions are split into a number of subbands, each of which can be separately sampled at the receiver using a lower rate ADC. For efficient use of spectrum, we do not allow guard bands between adjacent subbands, hence the receiver signal processing must account for intercarrier interference (ICI) across subbands as well as intersymbol interference (ISI) within a subband due to channel dispersion. We illustrate our ideas for short-range (100-200 meters), highly directional, outdoor 60 GHz links, as might be employed for wireless backhaul. Given the large coherence bandwidth of the sparse multipath channels typical of such links that we consider, reliable performance requires spatial diversity, in addition to the beamforming required to close the link. We therefore consider one transmit and two receive antenna arrays, each with 4×4 elements. We investigate linear equalization strategies corresponding to different combinations of: (a) combining samples from both arrays/choosing the stronger array and (b) equalizing the subbands independently/jointly. We find that exploiting the spatial diversity completely by combining samples from both arrays is critical for combating fading and inter carrier interference.**

I. Introduction

The availability of large amounts of unlicensed spectrum in the 60 GHz band (57-64 GHz in the United States), along with advances in silicon realizations of millimeter (mm) wave radio frequency integrated circuits (RFICs), open up the prospect of commercially viable multiGigabit wireless networks. Building transceivers for the mass market, however, requires that we take advantage of the digital signal processing enabled by Moore's law. A key bottleneck in doing this is the cost and power consumption of ADCs at high sampling rates. In this paper, we investigate how to circumvent this bottleneck for channel dispersion compensation for an outdoor 60 GHz link. Such links might be employed, for example, for wireless backhaul in a picocellular infrastructure, and might operate over ranges of 100-200 m, for which propagation losses due to oxygen absorption (characteristic of the 60 GHz band) and rain can be accommodated within a reasonable link budget.

Standard DSP-based approaches to channel dispersion using time-domain equalization or OFDM both require high-speed ADCs with large dynamic range and high precision: OFDM has an inherently large Peak-to-Average Power Ratio (PAPR), while multipath propagation creates large dynamic range even for singlecarrier transmission. High speed, high-precision ADCs based on conventional architectures, such as flash ADCs, are too costly or power-hungry [14]. Time-interleaved ADCs [15] have been proposed as a solution: a high rate ADC is synthesized using a number of slower ADCs whose sampling times are staggered, thereby providing a power efficient option. However, even though the sub-ADCs operate at a lower rate, the sample-and-hold blocks in each of the sub-ADCs still need to operate over the entire signal bandwidth, leading to issues of bandwidth scalability. In this paper, we investigate Analog Multitone (AMT) as a solution to the ADC bottleneck: the idea is to transmit in parallel over a small number of subbands (significantly smaller than the number of subcarriers employed by OFDM), each of which can be sampled using a relatively low rate ADC after analog filtering at the receiver. There are two advantages in splitting the transmissions into a number of subbands (say M). First, since each subband is smaller by a factor of M and transmissions happen in parallel over different subbands, it suffices to sample each subband with an ADC that is M times slower (including the sample-and-hold block). Second, the equivalent channel seen by the symbols over small subbands is significantly shorter than the channel seen over the entire band. For example, we see from the top panel of Figure 1 that the channel over the entire band has 24 taps. However, when we split the entire band into 4 or 8 subbands, the channel in one of the subbands has only 8 and 6 taps respectively. As a result, the equalization complexity in each subband is reduced substantially, and simple equalizers can be implemented in parallel.

The AMT scheme considered here employs excess band-

[1]This research was supported in part by the National Science Foundation under grant CNS-0832154.

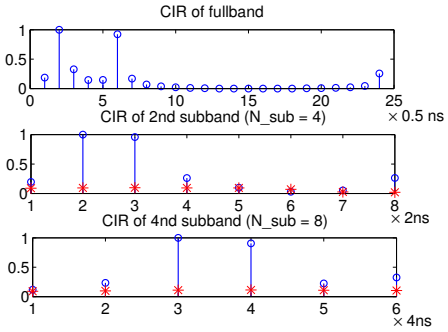

Fig. 1. Illustration of normalized channel impulse responses of a system of 2 GHz bandwidth at 60 GHz band with different number of subbands (The star marker denotes the ICI signal from the adjacent subband on the left).

width in each subband in order to limit peak amplitude and ISI, but does not provide guard bands between adjacent subbands, in order to avoid spectral wastage. This implies that we must combat ICI across subbands, in addition to the ISI within a subband due to channel dispersion. While AMT is a generic technique for decomposing high-rate channels into slower subchannels, we also need to combine it with features specific to 60 GHz. In particular, directional transmission and reception are critical to attaining the link budget at 60 GHz, and can be attained using compact printed circuit antenna arrays; we therefore consider beamforming with 4×4 antenna arrays in our modeling and performance evaluation. The relatively large coherence bandwidth for the sparse multipath channel induced by highly directional links implies that frequency diversity may not be enough to combat multipath fading; we therefore allow for spatial diversity at the receiver.

Contributions: We propose an Analog Multitone scheme for transmissions over dispersive channels spanning 2 GHz of bandwidth in the millimeter wave band. We consider a system with a 4×4 transmit array, and two 4×4 receive arrays. The arrays at the transmitter and receiver beamform towards each other along the Line-of-Sight (LoS) path (for simplicity, we do not consider spatial multipath combining or suppression). We derive an equivalent channel between the transmitter and the receivers that accounts for the beamforming patterns and the physical multipath channel, consisting of reflections off a nearby wall and the ground in addition to the LoS path. We split the transmissions into four or eight subbands and investigate four linear equalization strategies for demodulating each subband. These strategies are based on different combinations of the following choices: (a) Combine samples from both arrays optimally or choose samples from the array that sees the stronger channel in the subband and (b) Treat the interference from adjacent subbands as noise or exploit the structure of the interference from adjacent subbands. While we consider two receive arrays in order to provide spatial diversity, we find that the additional degrees of freedom provided by combining samples from both arrays provides much better interference suppression (avoiding error floors) than using only samples from the array which sees a stronger channel.

Related work: The concept of analog multitone was proposed nearly four decades ago, but was rendered obsolete by the emergence of OFDM. However, it was revived recently for supporting high data rates ($10 - 20$ Gbps) over backplane links [1] [2]. These systems allocate substantial guard bands between the different subbands, thereby simplifying the equalizer, but reducing the spectral efficiency. In contrast, we let the subbands overlap and account for ICI as well as ISI, and include features (such as beamforming and spatial diversity) specific to the wireless application at hand. A channelized digital receiver for ultra wide band (UWB) signals was proposed in [3]. The receiver employs several low-rate ADCs, each sampling in a small subband, but the transmission is over the entire band, hence received samples from different subbands need to be pooled for equalization, unlike our system, where equalization for each subband can be performed in parallel. The idea of splitting the transmission into subbands with zero guard band has been investigated before in cosine modulated multitone (CMT) systems [4], but this system, which is designed for flat fading (rather than frequency selective fading as considered here) discards half the available degrees of freedom in order to avoid ICI. Our own prior investigation of 60 GHz outdoor channels [5] [6] motivates the spatial diversity approach considered here, but focused on narrowband transmission, as opposed to the wideband, frequency-selective system investigated here.

II. System Model

We provide an example link budget, and then derive an equivalent channel model (for a typical 60 GHz multipath channel) for fixed transmit and receive beamforming weights. This is then used to set up a complex baseband model for the AMT scheme.

A. Link Budget and Channel Model

Link Budget: We consider transmission and reception using 4×4 arrays, where each element in the array is a microstrip antenna with a directivity gain of 7 dBi and the spacing between adjacent elements is $\lambda/2 = 2.5$mm. Since a 4×4 array provides a 12dB beamforming gain, the maximum allowable transmit power is 21dBm (after accounting for the directivity gain) [7]. This requires only 9dBm power output from each of the 16 power amplifiers, and is sufficient to support high data rate links across distances of 200m: for example, we can transmit data at 4 Gbps using using QPSK modulation over a bandwidth of 2GHz, after budgeting for an oxygen absorption loss of 16dB/km, a link margin of 5dB and a noise figure of 5dB.
Beamforming Weights: We consider transmission from one 4×4 array to a receiver with two such arrays, with the receive arrays being separated by a few wavelengths. The arrays are mounted on top of lampposts and the transmit and receive arrays are separated by 100s of meters. We choose the transmit and receive phases as in [8]: (a) the phases at the receive antennas are chosen so that each array beamforms to the center of the transmit array and (b) the phases at the transmit elements are chosen so that the transmitter beamforms to the midpoint of the line joining the centers of the two receive arrays.

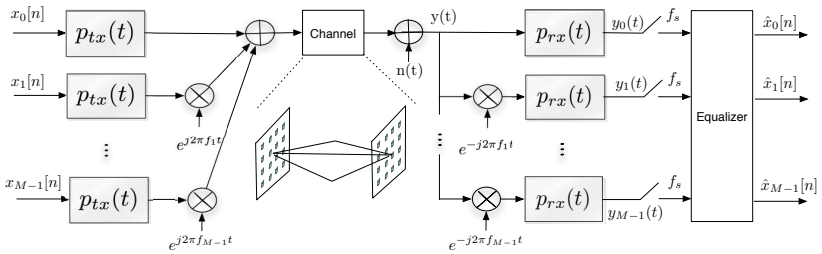

Fig. 2. Block diagram of the analog multitone system (only one of the two receive arrays is shown due to lack of space).

Equivalent channel model: The channel between the transmit and receive arrays consists of reflections from the ground and a nearby wall in addition to the LoS path. Suppose that there are L reflected paths and an LoS path (which we index to be the 0th path). The channel is then given by

$$h(t) = \sum_{l=0}^{L} g_{prop}[l] g_{BF}^{tx}[l] g_{BF}^{rx}[l] \delta(t - t_l), \tag{1}$$

where $g_{prop}[l], g_{BF}^{tx}[l], g_{BF}^{rx}[l]$ and t_l denote the propagation loss, beamforming gain at the transmitter, beamforming gain at the receiver and the propagation delay along the lth path respectively. We now specify each of these terms explicitly.

The propagation term along the LoS path is given by

$$g_{prop}[0] = \frac{\lambda}{4\pi R_0} e^{-\frac{K_p R_0}{2}} e^{-j\frac{2\pi R_0}{\lambda}}, \tag{2}$$

where R_0 is the distance along the LoS path and $K_p = 0.0016 \ln 10$ is the oxygen absorption (16 dB/km) at 60 GHz. The propagation term along the lth reflected path is similar (substituting R_l for R_0), except that also we need to include a multiplicative factor A_l to account for the reflection coefficient.

Consider the beamforming gain $g_{BF}^{tx}[0]$ at the transmitter along the LoS path. Assuming that this path makes angles (θ_{t0}, ϕ_{t0}) with the normal of the transmit array and one of the sides of the array respectively, the beamforming gain at the transmitter is given by

$$g_{BF}^{tx}[0] = \rho_{t0} \sqrt{N_t}, \tag{3}$$

where ρ_{t0} is the directivity gain of an antenna element along (θ_{t0}, ϕ_{t0}) and N_t is the number of elements in the transmit array. Analogously, the beamforming gain at the receiver $g_{BF}^{rx}[0] = \rho_{r0}\sqrt{N_r}$, where ρ_{r0} is the directivity gain of an antenna element along the receive direction (θ_{r0}, ϕ_{r0}) and N_r is the number of receive antenna elements.

Next, we specify the beamforming gains at the transmitter along the lth path. Let us denote the propagation delay from the ith transmit element to the center of the receive array along the lth path by d_{il}. Then, the beamforming gain at the transmitter along this path is given by

$$g_{BF}^{tx}[l] = \sqrt{\frac{\rho_{tl}}{N_t}} \sum_{i=1}^{N_t} e^{-j(2\pi f_c (d_{il} - d) + \beta_i)}, \tag{4}$$

where ρ_{tl} is the directivity gain along the lth path (θ_{tl}, ϕ_{tl}), d is the propagation delay from the reference element to the center of the receive array and $\{\beta_i\}$ are the beamforming weights. The beamforming gain at the receiver $g_{BF}^{rx}[l]$ can be computed analogously, but we omit an explicit expression owing to a lack of space.

For concreteness, we also specify the antenna patterns to compute the directivity gains along different paths. The normalized microstrip antenna element gain along the direction (θ, ϕ) is given by [9]:

$$\rho(\theta, \phi) = (\cos^2\theta \sin^2\phi + \cos^2\phi) \left| \cos(\pi v_x) \frac{\sin(\pi v_y)}{\pi v_y} \right|^2, \tag{5}$$

where $v_x = L \sin\theta/\lambda$ and $v_y = W \sin\theta/\lambda$, with L and W being the length and width of the microstrip antenna patch respectively. We choose $L = W = 0.5\lambda/\sqrt{\epsilon_r}$, with the relative permittivity of the dielectric substrate $\epsilon_r = 2.17$([10]).

B. Complex Baseband Model

Figure 2 shows a complex baseband model of the system. We split the transmission into M subbands. The symbols in the mth subband $\{x_m[n]\}$ pass through a transmit filter $p_{tx}(t)$ (square-root raised cosine) and are then upconverted to a frequency $f_m = f_c + m\Delta f, m = 0, 1, \ldots, M-1$ where Δf is the spacing between adjacent subbands. To achieve high bandwidth efficiencies, we allow the different subcarrier bands to overlap as shown in Figure 3. At the receiver, we recover the symbols from the mth subband by downconverting it to baseband, passing it through a receive filter $p_{rx}(t)$ (also square-root raised cosine) and sampling each subband at its Nyquist rate. We then pass these samples through an equalizer to eliminate the intercarrier interference before we estimate the symbols.

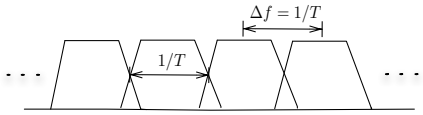

Fig. 3. Illustration of the subband allocation.

Denoting the channel seen by one of the receive arrays by $h(t)$, we derive an expression for the samples received from this array. The received signal before subband separation $y(t)$ is given by

$$y(t) = \sum_{m=0}^{M-1} \left(\sum_n x_m[n] p_{tx}(t - nT) e^{j2\pi f_m t} \right) \otimes h(t) + n(t) \tag{6}$$

where $\otimes$ denotes convolution, T is the symbol period and $n(t)$ is additive white Gaussian noise with two-sided power spectral density of $N_0/2$. The signal in the mth subband after the receive filter $y_m(t)$ consists of the following parts: the

desired transmitted signal from the mth subband (denoted by $y_{m\to m}(t)$) and the intercarrier interference signal from the $m-1^{th}$ and $m+1^{th}$ subbands (denoted by $y_{m-1\to m}(t)$ and $y_{m+1\to m}(t)$ respectively). Thus, we have:

$$y_m(t) = y_{m\to m}(t)+y_{m-1\to m}(t)+y_{m+1\to m}(t)+n_m(t), \quad (7)$$

where the noise term $n_m(t) = \left(n(t)e^{-j2\pi f_m t}\right) \otimes p_{rx}(t)$. Denoting the channel taps by $h(t) = \sum_{l=0}^{L} \alpha_l \delta(t-t_l)$, we can get explicit expressions for the contributions from different subbands as follows:

$$y_{m\to m}(t) = \sum_n \sum_{l=1}^{L} \alpha_l x_m[n] e^{-j2\pi f_m \tau_l} \left(p_{tx} \otimes p_{rx}\right)(t-nT-t_l),$$

$$y_{m-1\to m}(t) =$$

$$\sum_n \sum_{l=1}^{L} \alpha_l x_{m-1}[n] e^{-j2\pi f_m \tau_l} e^{-j2\pi \Delta f nT} \left(p^-_{tx} \otimes p_{rx}\right)(t-nT-t_l),$$

$$y_{m+1\to m}(t) =$$

$$\sum_n \sum_{l=1}^{L} \alpha_l x_{m+1}[n] e^{-j2\pi f_m \tau_l} e^{j2\pi \Delta f nT} \left(p^+_{tx} \otimes p_{rx}\right)(t-nT-t_l),$$

with $p^-_{tx}(t) = p_{tx}(t)e^{-j2\pi\Delta f t}$ and $p^+_{tx}(t) = p_{tx}(t)e^{j2\pi\Delta f t}$. From these equations, we see that the symbols see a time invariant channel if we choose $T\Delta f = 1$.

We define $h_m(t) = \sum_{l=1}^{L} \alpha_l e^{-j2\pi f_m \tau_l}\delta(t-\tau_l)$. By sampling $y_m(t)$ at a frequency $1/T$, we obtain the discrete sequence $y_m[k]$:

$$\begin{aligned} y_m[k] &= \sum_n \big(x_m[n]p_m(kT-nT) + x_{m-1}[n]p^-_m(kT-nT) \\ &\quad + x_{m+1}[n]p^+_m(kT-nT)\big) + n_m[k], \end{aligned} \quad (8)$$

where $p_m(t) = p_{tx} \otimes h_m \otimes p_{rx}(t)$ and $p^-_m(t) = p^-_{tx} \otimes h_m \otimes p_{rx}(t)$ and $p^+_m(t) = p^+_{tx} \otimes h_m \otimes p_{rx}(t)$. The discrete channel seen by the symbol $x_m[n]$ is given by $(p_m[0], p_m[1], \ldots)$, where $p_m[i] = p_m(iT)$. The channels seen by the symbols from the $m-1^{th}$ and $m+1^{th}$ bands are defined analogously, with p^-_m and p^+_m taking the place of p_m.

We truncate the channel response at a point where its samples are 40dB below the largest sample and denote the resulting length by v. In matrix-vector notation, the received samples in the mth subband, denoted by $\mathbf{y}_m[n]$, are given by

$$\begin{aligned} \mathbf{y}_m[n] &= \mathbf{H}_{m,m}\mathbf{x}_m[n] + \mathbf{H}_{m,m-1}\mathbf{x}_{m-1}[n] \\ &+ \mathbf{H}_{m,m+1}\mathbf{x}_{m+1}[n] + \mathbf{n}_m[n], \end{aligned} \quad (9)$$

where

$$\mathbf{H}_{m,m} = \begin{bmatrix} p_m[0] & \ldots & p_m[v] & 0 & 0 & 0 \\ 0 & p_m[0] & \ldots & p_m[v] & 0 & 0 \\ 0 & 0 & \ldots & \ldots & \ldots & 0 \\ 0 & 0 & 0 & p_m[0] & \ldots & p_m[v] \end{bmatrix}^T,$$

$\mathbf{x}_m[n] = [\cdots x_m[n-1], x_m[n], x_m[n+1], \cdots]^T$, $\mathbf{n}_m[n] = [\cdots n_m[n-1], n_m[n], n_m[n+1], \cdots]^T$, and $\mathbf{H}_{m,m-1}, \mathbf{H}_{m,m+1}$ are defined in a manner similar to $\mathbf{H}_{m,m}$ with p^-_m and p^+_m in place of p_m respectively.

The samples from the mth subband of the other receive array satisfy a similar model with a different set of channel matrices.

III. Equalization Schemes

In this section, we propose four schemes, with varying levels of complexity to cancel the ICI and ISI. These four schemes arise by considering different combinations of two choices:

• *Selection or Combining:* While demodulating subband m, we use samples from both arrays in the *combining* scheme. On the other hand, in the *selection* scheme, we only use the samples from the array that sees the stronger channel response. Specifically, denoting the channel response at array i by $(p^{(i)}[0], p^{(i)}[1], \ldots, p^{(i)}[v])$, we choose samples from the array that has a larger value of $\sum_{j=0}^{v} |p^{(i)}[j]|^2$. A block diagram of the selection schemes is shown in Figure 4.

• *Independent or Joint:* In the *independent* mode, we treat the interference from subbands $m-1$ and $m+1$ as noise while designing an equalizer for subband m. In the *joint* mode, we exploit the structure of the interference from subbands $m-1$ and $m+1$ while designing the equalizer. We now explain the models for each of these schemes in detail.

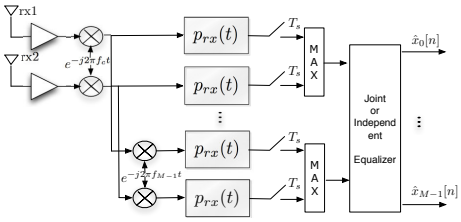

Fig. 4. Block diagram of ISEL or JSEL scheme.

Independent Selection scheme (ISEL): Suppose that we are demodulating subband m. We use a superscript s to denote the samples and the channel matrices from the "selected" (or, "stronger") array (as $\mathbf{y}^s_m[n], \mathbf{H}^s_{m,m}, \mathbf{H}^s_{m,m-1}, \mathbf{H}^s_{m,m+1}$ respectively). Treating the interference from adjacent bands as noise in (9), we get the model

$$\mathbf{y}^s_m[n] = \mathbf{H}^s_{m,m}\mathbf{x}_m[n] + \mathbf{n}'_m[n], \quad (10)$$

where the noise covariance $\mathbb{E}\left(\mathbf{n}'_m[n]\mathbf{n}'^H_m[n]\right) = \sigma^2\mathbb{I} + \sigma_x^2\mathbf{H}^s_{m,m-1}(\mathbf{H}^s_{m,m-1})^H + \sigma_x^2\mathbf{H}^s_{m,m+1}(\mathbf{H}^s_{m,m+1})^H$, with $\sigma^2 = N_0/2$ and σ_x^2 denoting the transmit power in each symbol.

Joint Selection scheme (JSEL): In each of the subbands $m-1, m$ and $m+1$, we choose samples from the antenna array that sees the stronger channel in the respective subband. In this case, we have the model

$$\begin{bmatrix} \mathbf{y}^s_{m-1}[n] \\ \mathbf{y}^s_m[n] \\ \mathbf{y}^s_{m+1}[n] \end{bmatrix} = G_{JS} \begin{bmatrix} \mathbf{x}_{m-1}[n] \\ \mathbf{x}_m[n] \\ \mathbf{x}_{m+1}[n] \end{bmatrix} + \begin{bmatrix} \mathbf{n}^s_{m-1}[n] \\ \mathbf{n}^s_m[n] \\ \mathbf{n}^s_{m+1}[n] \end{bmatrix}, \quad (11)$$

where $G_{JS} = \begin{bmatrix} \mathbf{H}^s_{m-1,m-1} & \mathbf{H}^s_{m-1,m} & \underline{\mathbf{0}} \\ \mathbf{H}^s_{m,m-1} & \mathbf{H}^s_{m,m} & \mathbf{H}^s_{m,m+1} \\ \underline{\mathbf{0}} & \mathbf{H}^s_{m+1,m} & \mathbf{H}^s_{m+1,m+1} \end{bmatrix}$.

Note that we are ignoring the contributions to $\mathbf{y}^s_{m-1}[n]$ and $\mathbf{y}^s_{m+1}[n]$ from the transmissions in the $m-2^{th}$ and $m+2^{th}$ subbands respectively.

Independent Combining scheme (ICOM): We use samples from subband m from both the arrays, but treat the interference from subbands $m-1$ and $m+1$ as noise. We use the superscript (i) to denote the samples collected from array i and the channel matrix seen by array i. Thus, we have the model

$$\begin{bmatrix} \mathbf{y}_m^{(1)}[n] \\ \mathbf{y}_m^{(2)}[n] \end{bmatrix} = \begin{bmatrix} \mathbf{H}_{m,m}^{(1)} \\ \mathbf{H}_{m,m}^{(2)} \end{bmatrix} \mathbf{x}_m[n] + \begin{bmatrix} \boldsymbol{\eta}_m^{(1)} \\ \boldsymbol{\eta}_m^{(2)} \end{bmatrix}, \quad (12)$$

where

$$\begin{bmatrix} \boldsymbol{\eta}_m^{(1)} \\ \boldsymbol{\eta}_m^{(2)} \end{bmatrix} = \mathbf{K}_{m-1}\mathbf{x}_{m-1}[n] + \mathbf{K}_{m+1}\mathbf{x}_{m+1}[n] + \begin{bmatrix} \mathbf{n}_m^{(1)}[n] \\ \mathbf{n}_m^{(2)}[n] \end{bmatrix},$$

and $\mathbf{K}_{m-1}$ stacks $\mathbf{H}_{m,m-1}^{(1)}$ above $\mathbf{H}_{m,m-1}^{(2)}$ and $\mathbf{K}_{m+1}$ stacks $\mathbf{H}_{m,m+1}^{(1)}$ above $\mathbf{H}_{m,m+1}^{(2)}$. From this equation, we obtain the covariance of the noise to be $\sigma_x^2\left(\mathbf{K}_{m-1}\mathbf{K}_{m-1}^H + \mathbf{K}_{m+1}\mathbf{K}_{m+1}^H\right) + \sigma^2\mathbb{I}$.

Joint Combining scheme (JCOM): We use all the available information (samples from both arrays from subbands $m-1, m$ and $m+1$) while demodulating subband m, giving us the model

$$\begin{bmatrix} \mathbf{y}_{m-1}^{(1)}[n] \\ \mathbf{y}_{m-1}^{(2)}[n] \\ \mathbf{y}_m^{(1)}[n] \\ \mathbf{y}_m^{(2)}[n] \\ \mathbf{y}_{m+1}^{(1)}[n] \\ \mathbf{y}_{m+1}^{(2)}[n] \end{bmatrix} = G_{JC} \begin{bmatrix} \mathbf{x}_{m-1}[n] \\ \mathbf{x}_m[n] \\ \mathbf{x}_{m+1}[n] \end{bmatrix} + \begin{bmatrix} \mathbf{n}_{m-1}^{(1)}[n] \\ \mathbf{n}_{m-1}^{(2)}[n] \\ \mathbf{n}_m^{(1)}[n] \\ \mathbf{n}_m^{(2)}[n] \\ \mathbf{n}_{m+1}^{(1)}[n] \\ \mathbf{n}_{m+1}^{(2)}[n] \end{bmatrix}, \quad (13)$$

where $G_{JC} = \begin{bmatrix} \mathbf{H}_{m-1,m-1}^{(1)} & \mathbf{H}_{m-1,m}^{(1)} & \mathbf{0} \\ \mathbf{H}_{m-1,m-1}^{(2)} & \mathbf{H}_{m-1,m}^{(2)} & \mathbf{0} \\ \mathbf{H}_{m,m-1}^{(1)} & \mathbf{H}_{m,m}^{(1)} & \mathbf{H}_{m,m+1}^{(1)} \\ \mathbf{H}_{m,m-1}^{(2)} & \mathbf{H}_{m,m}^{(2)} & \mathbf{H}_{m,m+1}^{(2)} \\ \mathbf{0} & \mathbf{H}_{m+1,m}^{(1)} & \mathbf{H}_{m+1,m+1}^{(1)} \\ \mathbf{0} & \mathbf{H}_{m+1,m}^{(2)} & \mathbf{H}_{m+1,m+1}^{(2)} \end{bmatrix}$.

In all these cases, the general model we have is

$$\mathbf{Y} = \mathbf{U}\mathbf{s} + \mathbf{n} \quad (14)$$

where the noise $\mathbf{n}$ is complex Gaussian with a covariance matrix $\mathbf{C}$. Let us denote the entries of $\mathbf{s}$ by $(s_0, s_1, s_2, \ldots)$ and suppose that we wish to estimate s_0. Denoting the corresponding columns of $\mathbf{U}$ by $\{\mathbf{u}_i\}$, we can rewrite the model in (14) as

$$\mathbf{Y} = s_0\mathbf{u}_0 + \sum_{i\neq 0} s_i\mathbf{u}_i + \mathbf{n}. \quad (15)$$

The MMSE estimate of s_0 is given by [13]

$$\hat{s}_0 = \mathbf{w}^H\mathbf{Y} = \left(\mathbf{R}^{-1}\mathbf{p}\right)^H\mathbf{Y}, \quad (16)$$

where $\mathbf{R} = E\{\mathbf{Y}\mathbf{Y}^H\} = \sigma_x^2\mathbf{U}\mathbf{U}^H + \mathbf{C}$ and $\mathbf{p} = E\{s_0^*\mathbf{Y}\} = \sigma_x^2\mathbf{u}_0$. The effective SINR at the output of the equalizer is given by

$$\text{SINR} = \frac{\sigma_x^2|\mathbf{w}^H\mathbf{u}_0|^2}{\sigma_x^2\sum_{i\neq 0}|\mathbf{w}^H\mathbf{u}_i|^2 + \mathbf{w}^H\mathbf{C}\mathbf{w}} \quad (17)$$

and we use this to compute the bit error rate.

IV. Simulation Results

We simulate links with a range of 200m and a bandwidth of 2 GHz. We consider one reflection each off a nearby wall and street in addition to the LoS path. The distance to the wall r_{wall} is uniformly distributed in $[4\text{m}, 20\text{m}]$ and the distance to the street is uniformly distributed in $[5\text{m}, 8\text{m}]$. The reflections result in a maximum delay spread of 13ns (26 symbol periods). We choose the reflection coefficients for the street and the wall based on the measurements in [11] [12]. We use square root raised cosine filters at the transmitter and the receiver with rolloff factors of 0.2. We split the transmissions into either 4 or 8 subbands and use QPSK modulation in each band with the receive SNR along the LoS path being 11 dB.

Array separation: We investigate the performance of the ISEL scheme with varying distances between the receive arrays with the goal of choosing a "good" value for the array separation. At the receiver, we consider two arrays separated by $2\lambda - 8\lambda$ (in both the horizontal and vertical directions). We use the ISEL scheme with 21 equalizer taps and plot the CDF of the SINR from (17) in Figure 5. For 4-subband transmission, we see that the performance with array separations of 4λ, 6λ and 8λ are nearly identical. Similarly, for 8-subband transmission, array separations of 6λ and 8λ work well. In the following simulations, we set the array separation to be 6λ (in both directions) since it works well with both 4 and 8-subband transmissions.

Value of multiple arrays: We investigate the SINR at the output of the equalizer for different schemes as function of the number of equalizer taps per subband per array, which we denote by N_{taps}. Thus, the total number of equalizer taps for JCOM, JSEL, ICOM, ISEL are $6N_{taps}$, $3N_{taps}$, $2N_{taps}$, and N_{taps} respectively. We consider a scenario with a large delay spread (r_{wall} = 20 m and r_{street} = 8 m) and assume that the channel is known perfectly. We average the SINR from (17) over all the subbands, except for the ones at the edges (bands 2 and 3 for the 4-subband system; bands 2-7 for the 8 subband system). We plot the results in Figure 6 and make the following observations:

- The performance with 8 subbands is significantly better than that with 4 subbands for the ICOM, JSEL and ISEL schemes (for JCOM, the performance is similar when the number of equalizer taps is large). Of course, we need twice as many equalizers for the 8-subband transmission when compared to 4-subband transmission.
- The SINR achieved with ICOM is 4 dB higher than that with JSEL even though it uses *fewer* equalizer taps than JSEL ($2N_{taps}$ vs. $3N_{taps}$). Thus, it is essential to combine signals from both arrays, rather than simply select the stronger one, to combat frequency selective fading and ICI.
- In terms of the SINR achieved with a large number of equalizer taps, we can rank the schemes as JCOM>ICOM>JSEL>ISEL with the ratios of their complexities being $6:2:3:1$.

BER performance: We investigate the performance of the different schemes when the channels are not known perfectly and

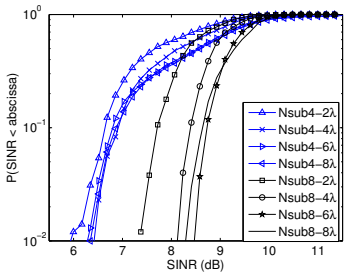

Fig. 5. The CDF of the obtained SINR of the ISEL scheme with 4 and 8 subband channels for different antenna separations from 2λ to 8λ.

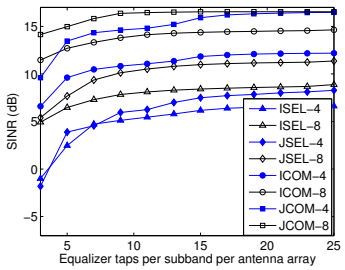

Fig. 6. SINR as a function of equalizer taps per subband per antenna array for four schemes with 4 subbands and 8 subbands.

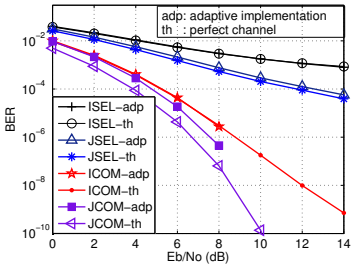

Fig. 7. BER as a function of E_b/N_0 (along the LoS path) for different schemes with both adaptive implementation and calculation using perfect channel knowledge.

the equalizer taps are estimated from a training sequence. We compute the equalizer taps in the mth subband by adaptively estimating $\mathbf{R}_m$ and $\mathbf{p}_m$ as $\mathbf{R}_m = \frac{1}{N_{train}} \sum_i^{N_{train}} \mathbf{Y}_m[i]\mathbf{Y}_m^H[i]$ and $\mathbf{p}_m = \frac{1}{N_{train}} \sum_i^{N_{train}} \mathbf{Y}_m[i]x_m^*[i]$ from training symbols $\{x_m[i], i = 1, 2, \ldots, N_{train}\}$ and then using them in (16). We simulate the performance by transmitting 10^5 symbols of which 1000 symbols are used for training. We use 21 equalizer taps per subband per antenna array and consider 100 channel realizations with different distances to the wall r_{wall} and the street r_{street}. We plot the average BER from simulations in the 4th subband of the 8-subband system in Figure 7. We also plot the BER assuming perfect channel knowledge $Q(\sqrt{\text{SINR}})$, where the SINR is given by (17). We make the following observations:

- Both ISEL and JSEL have relatively high error floors (8×10^{-3} and 5×10^{-5} at 14 dB respectively). This happens because a finite length MMSE equalizer operating on symbol-rate samples does not have sufficient dimensions to suppress the ISI completely (even ignoring ICI) [13]. On the other hand, using samples from both arrays in ICOM and JCOM essentially provides a fractionally spaced equalizer with sufficient degrees of freedom to suppress interference completely, thereby eliminating the error floor.
- Comparing the combining strategies (the adaptive implementation curves), we see that JCOM provides a 1 dB gain over ICOM (at $E_b/N_0 = 8$ dB), while incurring thrice the complexity.
- With JCOM and JSEL, we have to estimate a larger number of equalizer taps in comparison to ICOM and ISEL. The errors in estimating the equalizer taps result in a slightly larger BER than predictions assuming perfect channel knowledge. We see that the simulated performance is about 0.4 dB and 0.9 dB worse than the theoretical prediction for JSEL and JCOM respectively.

V. Conclusion

Analog Multitone is a general technique for scaling communication systems to large bandwidths while sidestepping the ADC bottleneck. In this paper, we have shown that it can be used in conjunction with beamforming and spatial diversity for robustly attaining multiGigabit rates on outdoor 60 GHz links. Separate linear equalization for each subband suffices to avoid performance floors, as long as the additional degrees of freedom provided by using samples from both receive arrays are used (i.e., the ICOM scheme provides perhaps the best complexity/performance tradeoff among the schemes considered here).

Interesting topics for future investigation include exploring potential performance gains from decision feedback, oversampling, and more intelligent beamforming (e.g., MMSE adaptation for multipath combining and suppression). It is also of interest to study performance under more detailed channel models including multiple reflections, as well as to explore similar approaches for indoor environments.

References

[1] A. Amirkhany, V. Stojanovic, and M. Horowitz. Multi-tone signaling for high-speed backplane electrical links. in *Proc. IEEE GLOBECOM' 04*, volume 2, 2004.

[2] A. Amirkhany, A. Abbasfar, , and et al., A 24 Gb/s software programmable analog multi-tone transmitter. *IEEE Journal of Solid-State Circuits*, 43(4):999–1009, 2008.

[3] W. Namgoong. A channelized digital ultrawideband receiver. *IEEE Transactions on Wireless Communications*, 2(3):502–510, 2003.

[4] P. Amini, R. Kempter, and B. Farhang-Boroujeny. A comparison of alternative filterbank multicarrier methods for cognitive radio systems. in *Software Defined Radio Technical Conference*, 2006.

[5] H. Zhang, S. Venkateswaran, and U. Madhow. Channel modeling and MIMO capacity for outdoor millimeter wave links. in *Proc. IEEE WCNC 2010*, Apr. 2010.

[6] H. Zhang and U. Madhow. Statistical modeling of fading and diversity for outdoor 60 GHz channels. in *Proc. International Workshop on mmWave Communications (mmCom10)*, 2010.

[7] S. Yong and C. Chong. An overview of multigigabit wireless through millimeter wave technology: potentials and technical challenges. *EURASIP J. on Wireless Communications and Networking*, 2007.

[8] M. Park and P. Gopalakrishnan. Analysis on spatial reuse and interference in 60-GHz wireless networks *IEEE Journal on Selected Areas in Communications*, 2009.

[9] S. Orfanidis. Electromagnetic Waves and Antennas, Rutgers University, 2008.

[10] J. Akkermans and M. Herben. Planar beam-forming array for broadband communication in the 60 GHz band. in *The Second European Conference on Antennas and Propagation, EuCAP 2007*, IET, 2007.

[11] L. Correia and P. Frances. Estimation of materials characteristics from power measurements at 60 GHz. in *Proc. IEEE 7th Int. Conf. PIMRC*, pages 510–513, Oct. 1994.

[12] K. Sato, T. Manabe, J. Polivka, T. Ihara, Y. Kasashima, and K. Yamaki. Measurement of the complex refractive index of concrete at 57.5 GHz. *IEEE Transactions on Antennas and Propagation*, 44(1):35–40, 1996.

[13] U. Madhow. *Fundamentals of Digital Communication*. Cambridge University Press, 2008.

[14] B. Le, T.W. Rondeau, J.H. Reed, and C.W. Bostian Analog-to-digital converters *IEEE Signal Processing Magazine*, 22(6):69–77, 2005.

[15] S. Ponnuru, M. Seo, U. Madhow, and M. Rodwell Joint mismatch and channel compensation for high-speed OFDM receivers with time-interleaved ADCs *IEEE Transactions on Communications*,58(8):2391–2405,2010.